

An adaptive semi-supervised Fuzzy GrowCut algorithm to segment masses of regions of interest of mammographic images

Filipe R. Cordeiro^a, Wellington P. Santos^{b,*}, Abel G. Silva-Filho^a

^a Informatics Center, Federal University of Pernambuco, Brazil

^b Department of Biomedical Engineering, Federal University of Pernambuco, Brazil



ARTICLE INFO

Article history:

Received 10 June 2015

Received in revised form 4 August 2015

Accepted 23 November 2015

Available online 12 December 2015

Keywords:

Breast cancer

Mass detection

Mammography image analysis

Biomedical image segmentation

GrowCut algorithm

ABSTRACT

According to the World Health Organization, breast cancer is the most common cancer in women worldwide, becoming one of the most fatal types of cancer. Mammography image analysis is still the most effective imaging technology for breast cancer diagnosis, which is based on texture and shape analysis of mammary lesions. The GrowCut algorithm is a general-purpose segmentation method based on cellular automata, able to perform relatively accurate segmentation through the adequate selection of internal and external seed points. In this work we propose an adaptive semi-supervised version of the GrowCut algorithm, based on the modification of the automaton evolution rule by adding a Gaussian fuzzy membership function in order to model non-defined borders. In our proposal, manual selection of seed points of the suspicious lesion is changed by a semiautomatic stage, where just the internal points are selected by using a differential evolution algorithm. We evaluated our proposal using 57 lesion images obtained from MiniMIAS database. Results were compared with the semi-supervised state-of-the-art approaches BEMD, BMCS, Wavelet Analysis, LBI, Topographic Approach and MCW. Results show that our method achieves better results for circumscribed, spiculated lesions and ill-defined lesions, considering the similarity between segmentation results and ground-truth images.

© 2015 Elsevier B.V. All rights reserved.

1. Introduction

Breast cancer has become an increasing problem for women worldwide: according to the World Health Organization (WHO), it is the most common type of cancer in women, with increasing mortality, both for developed and underdevelopment countries, becoming one of the most fatal forms of cancer [1]. Nearly 1.7 million new cases were diagnosed in 2012, which represents about 12% of all new cancer cases and 25% of all cancers in women, with 522,000 deaths [2]. Breast cancer survival rates can vary between 80% in high-income countries, to below 40% in low-income ones [3]. The low survivability in some countries is related to the lack of screening programs which assist in the early detection of cancers. Early detection has an important impact on the successful treatment of cancer, once medical treatment becomes harder in late stages. One of the most effective methods for breast cancer analysis is digital mammography [4]. However, mammography visual understanding and analysis can be a hard task even to a specialist,

once such a procedure can be affected by image quality aspects, radiologist experience, and tumor shape.

After the beginning of breast cancer, the period until tumors become palpable, i.e. reaching a diameter around 1cm, is about 10 years [5]. During this period, breast imaging is essential, both for early detection and tumor monitoring. Correct evaluation of the tumor size takes an important role in the planning of the breast cancer treatment, avoiding mutilating surgeries, such as mastectomy [6]. Nevertheless, these methods depend substantially on the professional examiners experience [7]. Furthermore, image analysis and diagnosis are complex, mainly because of the large variability of cases. For these reasons, Mammography Computer-Aided Diagnosis (MCAD) has been playing an import role to assist radiologists and other related health professionals in improving the accuracy of their diagnoses. Consequently, traditional techniques in image processing have been applied in the medical field to make diagnosis less susceptible to errors through accurate identification of anatomic anomalies [8,9].

The size of the segmented tumor is a determinant factor in the mammogram diagnosis. It is very related to the malignancy of the tumor, where a difference of just a few centimeters in the maximum diameter can determine whether is necessary to do a surgery or not. However, it can be very difficult to detect the

* Corresponding author. Tel.: +55 81992336855.

E-mail addresses: frc@cin.ufpe.br (F.R. Cordeiro), [\(W.P. Santos\)](mailto:wellington.santos@ufpe.br), [\(A.G. Silva-Filho\)](mailto:agsf@cin.ufpe.br).

contour of the tumor accurately depending on several factors, such as tumor shape, density, size, location, and overall image quality. Some challenges in tumor segmentation include low contrast images, intensity levels with considerable variation across different regions, poor illumination, high noise levels, ill-defined contours, and masses not obviously detected [10].

The GrowCut algorithm is an interactive supervised segmentation method by which users can obtain feasible results by selecting just a few points from inside and outside the region of interest [11]. This feature makes GrowCut an interesting tool to segment objects of interest in medical images, because no other parameters are needed. The general-purpose GrowCut segmentation algorithm is based on cellular automata dynamics [11]. These cellular automata are associated to pixels, which are previously labeled at the stage of selecting points inside and outside the region of interest. Interaction between these cellular automata results image dynamic labeling. This interaction is governed by competitive rules, which are described in details in Section 3.1, in which GrowCut diagrams and pseudocode are presented. Consequently, the evolution of cellular automata depends on the selection of points internal and external to the object of interest, making possible good segmentation of relatively difficult objects with complex borders, in a process whose quality is highly dependent on user experience [11]. The higher the quality of points selection, i.e. the higher the user experience, the higher the quality of image segmentation results.

In this work we propose an adaptive fuzzy semi-supervised version of the GrowCut algorithm based on two basic modifications: (a) automatic selection of internal points using the differential evolution optimization algorithm, maximizing the minimum distance between these points and the minimum gray level of the associated pixels, in order to minimize the need of human intervention; (b) modification of cellular automata evolution rules by introducing Gaussian fuzzy membership functions, in order to make the algorithm able to deal with complex and non-defined mammary lesion borders. Results were generated using the MiniMIAS mammography image database, demonstrating that our approach could reach better results than using other state-of-the-art segmentation methods, regarding metrics that evaluate the similarity of lesion shapes to ground-truth results.

This paper is organized as following: in Section 2 we present related state-of-the-art works; in Section 3 we present a brief description of the GrowCut algorithm, details of the proposed method and methodology, a description of the image database MiniMIAS, and the metrics we employed to evaluate our proposal; in Section 4 we show some experimental results we obtained in comparison with the state-of-the-art segmentation methods; in Section 5 we discuss about the quality of the results; finally, in Section 6 we perform general conclusions, discuss other applications and perspectives of our proposal.

2. Related work

Recent works have provided good accuracy in identifying the location of tumors [12,13]. Ertas et al., for example, proposes the first demonstration of the use of multicellular neural networks lesion localization in magnetic resonance mammography [14,15], achieving good results. Jiji et al. [16] propose a scheme for predicting the real stage of breast cancer by retrieving the mammogram images from the past cases, achieving 87% classification rate. Sundaram et al. [17] propose the Histogram Modified Local Contrast Enhancement (HM-LCE) to adjust the level of contrast enhancement, which in turn gives the resultant image a strong contrast and also brings the local details present in the original image for more relevant interpretation. Nijad et al. [18] combine various enhancement methods and to segment breast region in order to

obtain better visual interpretation analysis and classification of mammogram masses. Oliver et al. [19] makes a review of state-of-the-art and shows that related works are divided into edge-based segmentation, region-based segmentation, and adaptive threshold methods.

In edge-based segmentation, it is difficult to determine the boundary of the tumor due to some ill-defined lesion edges. Region-based segmentation is considered more suitable for mass detection, since regions of tumor are usually brighter than their surrounding tissues, having almost uniform densities and fuzzy boundaries [10].

Recent studies for tumor segmentation have been successfully applied to region-based techniques for tumor segmentation. Lewis et al. [20] employ Watersheds to automatically segment tumor candidate regions, achieving an overall detection rate for mass tumors of 90%. However, the used metric of analysis was based only on tumor location, not on the quality of segmentation.

Eltoukhy and Faye [21] use an adaptive threshold technique, achieving 100% of sensitivity, with an average of 1.87% false positives, when applied to 188 images. However, the value of sensitivity varies depending on the false positive rate, and each work uses a different rate.

Hong proposes a Topographic Approach [22] of segmentation, based on the fact that suspicious regions are usually brighter than neighbor regions, with uniform densities. However, for most of cases, regions of lesion do not have well-defined contours. Due to this fact, seed-based techniques, i.e. techniques in which users label initial seeds, achieve better quality in the final segmentation. GrowCut technique has been applied to successfully segment medical images, such as kidney [23] and brain [24]. Cordeiro et al. [25] apply the classical GrowCut to segment masses in mammograms, obtaining good results in terms of quality of segmentation. Zen et al. [26] use a random-walk based segmentation, a method that also uses seeds provided by the user to achieve good segmentation results, but they do not provide quantitative analysis of the experimental results. Despite seed-based techniques have shown suitable performance for mass segmentation, they require a high level of specialist knowledge about the seed selection problem.

Unsupervised and semi-supervised techniques try to reduce the required specialist knowledge on tumor region. Ramathi et al. use Active Contours [27] to segment masses, achieving 86.85% of accuracy using an overlap measure between segment images and ground-truth. Chakraborty et al. apply Multilevel Threshold [28] combined with region growing to perform segmentation for well-defined edge contours. However, both techniques present difficulties at defining spiculated contours and ill-defined edges.

Pereira et al. [29] uses an approach bases on Wavelet Analysis, achieving 79.2% of precision, for craniocaudal and mediolateral mammographic views.

Berber et al. proposes a Breast Mass Contour Segmentation algorithm (BMCS), which uses an approach based on region growing, achieving 83.15 % of precision using the metric of Area Overlap Measure.

Jai-Andaloussi et al. [30] uses a bidimensional emperical mode decomposition (BEMD) method to segment mammography images achieving 83.96% of mean precision of segmenting masses of different classes of abnormality. As observed by Raman et al. [10], the results obtained with the related state-of-the-art works are significantly different. They are often based on visual subjective opinion with very little quantitative endorsement. Furthermore, most studies describe an accuracy of the techniques based only on the localization of the tumor and not on its shape and contour, very important aspects for accurate diagnoses. Most works discuss the quality of segmentation based on Area Overlap Measure or accuracy. However, a deeper analysis comparing the shape of segmented image and ground-truth is necessary to verify the quality of contour obtained. This work proposes a new approach based on

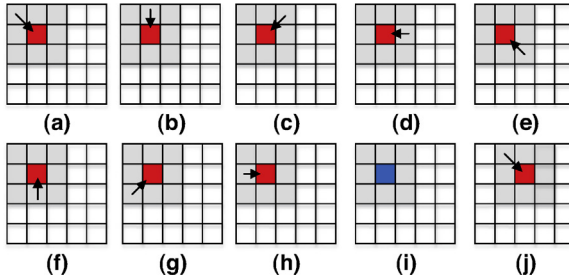


Fig. 1. The attack of a defender cell, in red, by its neighborhood, in grey. The defender cell assumes the label of the stronger neighbor. The process is repeated to all cells of the grid. (For interpretation of the references to color in this figure legend, the reader is referred to the web version of the article.)

automatic selection of seeds. We compared our proposal with other state-of-the-art techniques, analyzing the quality of segmentation of each technique based on shape metrics.

3. Materials and methods

3.1. Proposed model

Our proposal is based on a modification of the GrowCut algorithm [11], a general-purpose interactive segmentation algorithm able to segment objects with relatively complex borders by selecting adequate points internal and external to the region occupied by the object of interest. GrowCut is based on cellular automata dynamics [31], represented by grids of cells, where each cell can assume a finite number of states, varying according to neighborhood rules. Such cell neighborhood is composed by neighbor pixels defined according to Neumann and Moore neighborhood models [32], for instance. All cells update their states according to the same update rule, based on the configuration of neighbor cells.

The GrowCut technique uses the concept of seed pixels: users initially label a set of pixels associated to different classes and, taking into account the gray levels of these seeds, the algorithm tries to label all the pixels of the image. Each cell has a strength value and, at each iteration, the neighbor cells try to dominate this determined cell, changing its label. In case of a defender cell has a higher strength than its dominators, then its label persists the same. Otherwise, this specific cell inherits the label of the dominant cell. This process continues until the algorithm reaches convergence, i.e. label remain the same. Fig. 1 shows this process.

In Fig. 1, the defender cell is represented in red, while its neighborhood is shown in gray. Each neighbor of the defender cell tries to dominate the defender cell. This attack is based on the strength of each cell and the difference of intensity values between attacker and defender cell. From Fig. 1(a) to (h), it is shown that each neighbor attacks the defender cell. When an attacker cell successfully dominate the defender cell, the defender cell has the label of attacker cell cloned, but its new strength is based on the evolution update rule, which is described in this section. Fig. 1(i) illustrates the change of label of the defender cell. Fig. 1(j) shows the start of the process with other cell. This process is performed with all cells of the grid. The Evolution of the cells is performed through iterations, which in each iteration all cells os the grid act as defender cells being attacked by its neighborhood. Within the same iteration this process is performed in parallel. Fig. 2 shows the evolution of a cells domain in the GrowCut technique, in different iterations of the evolution process.

Fig. 2(a) shows the initial step, with two initial seed pixels. Each seed pixel have maximum value of strength because its assumed that the user is sure about the label of the pixel. In further iterations the seed pixels propagate its labels, and the cells dominated have

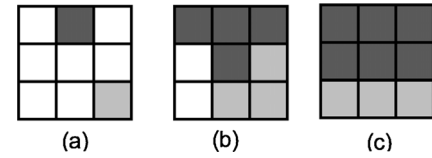


Fig. 2. GrowCut's cells evolution.

lower strength value, but inherits the label of the attacker. Pixels with no labels have strength zero, represented as the white cells in Fig. 2(b), and are easily dominated. The final step, in Fig. 2(c) shows a situation in which cells do not change its labels anymore and therefore the algorithm stops.

The GrowCut algorithm receives as input the image to be segmented and the label matrix with the labels provided by the user. The label provided by the user can be of two types: background label or object label, which corresponds to the regions outside and inside of the lesion. Initially the cell grid has cells with no labels associated. When the user determines the object and background labels of chosen cells, the labeled cells start to interact with its neighborhood. The GrowCut updating algorithm is described in pseudo-code of Algorithm 1.

Algorithm 1. GrowCut evolution rule

```

1: procedure GrowCutP,  $I$ 
2: for all  $p \in P$  do
3:   if  $l_p = l_{obj}$  or  $l_p = l_{bg}$  then
4:      $\Theta_p = 1$ 
5:   else
6:      $\Theta_p = 0$ 
7:   end if
8: end for
9: for all  $p \in P$  do
10:    $l_p^{t+1} \leftarrow l_p^t$ 
11:    $\Theta_p^{t+1} \leftarrow \Theta_p^t$ 
12:   for all  $q \in N(p)$  do
13:     if  $g(\|\vec{C}_p - \vec{C}_q\|_2) \cdot \Theta_q^t > \Theta_p^t$  then
14:        $l_p^{t+1} \leftarrow l_q^t$ 
15:        $\Theta_p^{t+1} \leftarrow g(\|\vec{C}_p - \vec{C}_q\|_2) \cdot \Theta_q^t$ 
16:     end if
17:   end for
18: end for
19: return  $l$ 
20: end procedure

```

Initially, for each cell p in a P space of cells, which corresponds to the pixels of the image, if the label value of cell p , represented as l_p was labeled by the user as an object label or background label, represented as l_{obj} and l_{bg} , respectively, the strength of cell p , represented as Θ_p , is equal to 1, otherwise is equal to 0. Next, for each cell p in a P space of cells, the previous states are copied, updating the label value of cell p in iteration $t + 1$, represented as l_p^{t+1} , and the strength value of cell p in iteration $t + 1$, as Θ_p^{t+1} . Subsequently, for each cell q belonging to the neighborhood of cell p , represented by $N(p)$, the update label condition is checked. In condition of line 5, \vec{C}_p and \vec{C}_q are intensity vectors of the pixels p and q in the grayscale space of colors, respectively, and Θ_q^t and Θ_p^t are values of strength of cells q and p in the iteration t . The function g , in line 7, is a decreasing monotonic function, represented by Eq. (1), which regulates the strength based on the attackers and defenders vectors of pixels. The $\max \|\vec{C}\|_2$ value of Eq. (1) represents the maximum value of vector of pixels between attackers and defenders cells.

$$g(x) = \frac{x}{\max \|\vec{C}\|_2} \quad (1)$$

Finally, the label and strength of cells are updated in case the domination rule is satisfied, and the process repeats until the algorithm converges.

In GrowCut, as in the majority of seed based techniques, the quality of segmentation depends directly on the positions of the initial seeds. Therefore, it depends on the user's knowledge to select appropriately seeds next to the edge of the object to be segmented. In case some seeds are initially labeled incorrectly, the algorithm may perform an undesired poor segmentation.

With our proposed modified GrowCut algorithm, we aim to reduce the need for initial specialist knowledge about the contour of the object of interest by reducing the effort of selection of seeds. Moreover, the proposed algorithm aims to be fault tolerant, being able to recover from incorrect seed selection.

In classical GrowCut, all the initial seeds selected by the user have maximum strength value, assigning high weights to seeds with incorrect labels. Unlike classical GrowCut, our modified GrowCut is based on the selection of seeds of only one class: the object of interest. We discard the selection of a background class because, from the seeds of the object of interest, we can estimate a frontier region separating object and background. Therefore, instead of assigning all the labeled cells with maximum strength, all the cells are initialized with zero strength, except the cell corresponding to the center of mass of input seeds. Hence, we assign the maximum value to the cell of the center of mass, once we assume it has a higher chance of being correct labeled. The initialization is performed according to the expressions of Eq. (2).

$$\forall p \in P, \quad l_p = 0, \quad \Theta_p = 0, \quad l_{cm} = l_{obj}, \quad \Theta_{cm} = 1, \quad (2)$$

where p is a cell in space P of cells, and l_p and Θ_p are the labels and strengths of cell p , respectively. Label and strength of the cell of the center of mass of the seeds are represented by l_{cm} and Θ_{cm} , respectively.

In our proposal, we also modified the update rule of GrowCut cells in a way that the attack of each cell is based in a region modeled by a Gaussian fuzzy membership function. The Gaussian function is a probability density function of a normal distribution, which can be represented, in two dimensions, based on the parameters of average and standard deviation. Fig. 3 (a) and (c) shows an example of Gaussian region, in two and three dimensions, respectively, where the regions in red indicates a higher frequency of data, which can also be interpreted as a higher chance of a data be present.

Fig. 3(b) shows a region of tumor of a digital mammography image, mapped in different levels of intensity. The regions in red represent the regions with higher intensities pixels, while the blue regions are the the regions with lower intensities. Fig. 3(d) shows the same tumor region, but in a three dimensional view.

As can be observed, the region of tumor has a behavior similiar to a Gaussian region. Consequently, the region of tumor described by a digital mammography image can be represented by a gaussian function. This does not mean that the contour of the tumor will be defined by the expression determined by the function but that the region where the tumor is located can be represented approximately by the function. The same can be observed in other images of tumor and in spiculated, circumscribed or ill-defined tumors, because the initial interest of the gaussian function is in the region where the tumor is located, and not in the definition of the edges. Based on the gaussian representation, it can be mapped by a membership function of presence of the tumor. Therefore, can be defined a fuzzy-gaussian membership region of a pixel to the region of tumor. This representation is useful to guide a seed based model, because it determines a model not only based on the initial seed points, but also on the membership region. The proposed model uses this representation.

In the proposed approach, the initial localization of seeds is enough to estimate a fuzzy-gaussian function. The strength of the

model will be equal to 1 if the pertinence of a determined cell to the background is higher than the pertinence of the same cell to the object. Otherwise, the strength of the model assumes the strength of the current cell. The update evolution rule of the GrowCut algorithm we propose is shown by the pseudo-code of Algorithm 2, where $\Theta_{M,p}^t$ and $\Theta_{M,q}^t$ are the model strengths for cells p and q , respectively, being represented by Eqs. (3)–(5), as following:

Algorithm 2 (ht). Modified GrowCut evolution rule

```

1: procedure ModifiedGrowCutP,  $I$ 
2:    $l_{cm} = l_{obj}$ 
3:    $\Theta_{cm} = 1$ 
4:   for all  $p \in P$  do
5:      $l_p^{t+1} \leftarrow l_p^t$ 
6:      $\Theta_p^{t+1} \leftarrow \Theta_p^t$ 
7:     Calculate  $\Theta_{M,p}^t$ 
8:   for all  $q \in N(p)$  do
9:     Calculate  $\Theta_{M,q}^t$ 
10:    if  $g(\|\tilde{C}_p - \tilde{C}_q\|_2) \cdot \Theta_{M,q}^t > \Theta_{M,p}^t$  then
11:      Calculate  $l_{M,p,q}^t$ 
12:       $l_p^{t+1} \leftarrow l_{M,p,q}^t$ 
13:       $\Theta_p^{t+1} \leftarrow g(\|\tilde{C}_p - \tilde{C}_q\|_2) \cdot \Theta_{M,q}^t$ 
14:    end if
15:   end for
16:   end for
17:   return  $I$ 
18: end procedure

```

$$\Theta_{M,i} = \begin{cases} 1, & \mu_{Bkg}(i) > \mu_{Obj}(i) \\ \Theta_i, & \mu_{Bkg}(i) \leq \mu_{Obj}(i) \end{cases}, \quad (3)$$

$$\mu_{Bkg}(i) = 1 - \mu_{Obj}(i), \quad (4)$$

$$\mu_{Obj}(i) = \exp\left(-\frac{(x_i - x_m)^2}{2\alpha_x s_x^2}\right) \exp\left(-\frac{(y_i - y_m)^2}{2\alpha_y s_y^2}\right), \quad (5)$$

where $\mu_{Bkg}(i)$ is the the fuzzy membership degree associated to the uncertainty of the i th cell belongs to the image background, whilst $\mu_{Obj}(i)$ is the the fuzzy membership degree associated to the uncertainty of the i th belongs to the object of interest. These fuzzy membership functions are Gaussian functions whose variables x_i and y_i correspond to the coordinates of the i th cell in the grid, whereas x_m and y_m are the coordinates of the center of mass for the initially selected seeds; s_x and s_y are the standard deviation of initial points, whilst α_x and α_y are the weights of tuning of the Gaussian function, empirically determined according to the problem of interest. The s_x and s_y are obtained calculating the standard deviation of the position of the points generated by the Differential Evolution algorithm.

The label of each q th cell, $l_{M,p,q}$, is updated according to the following expression of Eq. (6)

$$l_{M,p,q} = \begin{cases} l_p, & \mu_{Bkg}(q) > \mu_{Obj}(q) \\ l_q, & \mu_{Bkg}(q) \leq \mu_{Obj}(q) \end{cases}. \quad (6)$$

Table 1 presents a comparison between the classical version and our modified GrowCut algorithm.

The main difference between the classical GrowCut and our proposal is the consequent reduction of the effort to select seeds, once our approach requires users to choose just the points internal to the object of interest, because the background region is determined by the complement of the Gaussian fuzzy membership function responsible to regulate the strength and the label of each cell at the updating process. The introduction of Gaussian fuzzy membership functions whose parameters are determined by statistics of the selected points positions also make our proposal more fault-tolerant and, consequently, less dependent on user specialist

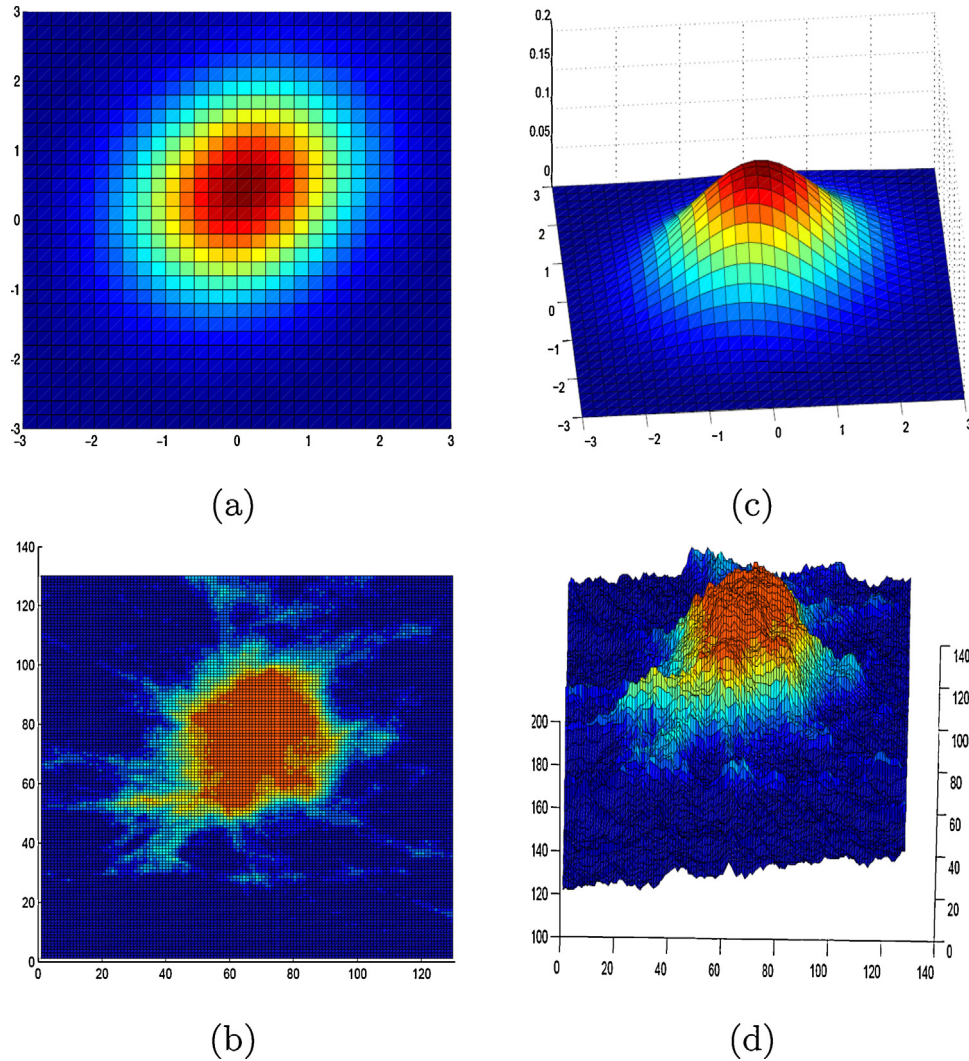


Fig. 3. (a) Gaussian region in two dimensions; (b) levels of intensity of a tumor region, in two dimensions; (c) Gaussian region in three dimensions; (d) levels of intensity of a tumor region, in three dimensions.

Table 1
Comparison between GrowCut and the proposed algorithm.

Characteristic	GrowCut	Modified GrowCut
Selection of seeds	Selection of seeds of object class and background class.	Selection of seed only of object class.
Initialization	All the seeds have strength value equal to 1, which is represented by line 4 of Algorithm 1 : $\Theta_p = 1$, where Θ_p is the strength of the seed point p . This is done for all seed points.	Only the cell corresponding to the center of mass of points has strength value equal to 1, which is represented in line 3 of Algorithm 2 : $\Theta_{cm} = 1$, where Θ_{cm} is the strength of the cell corresponding to the center of mass of the seed points.
Segmentation	Based on knowledge of seeds localization provided by the user.	Based on knowledge of seeds localization and in the Gaussian function that separates the region of foreground and background region.
Evolution rule	Based on difference of intensity values and strength of the attacking cell, represented in lines 14 and 15 of Algorithm 1 , described below: $\Theta_p^{t+1} \leftarrow g(\ \tilde{C}_p - \tilde{C}_q\ _2) \cdot \Theta_q^t$ where I_p , I_q , Θ_p and Θ_q are the labels and strengths of cells p and q respectively.	Based on difference of intensity values, strength of the attacking cell and on a fuzzy membership function, as represented in lines 11–13 of Algorithm 2 , Calculate $I_{M,p,q}^{t+1} \leftarrow I_{M,p,q}^t$ described below: $\Theta_p^{t+1} \leftarrow g(\ \tilde{C}_p - \tilde{C}_q\ _2) \cdot \Theta_q^t$ The values of $I_{M,p,q}$ and $\Theta_{M,q}$ are defined by Eqs. (3–6), as described below: $I_{M,p,q} = \begin{cases} I_p, & \mu_{Bkg}(q) > \mu_{Obj}(q) \\ I_q, & \mu_{Bkg}(q) \leq \mu_{Obj}(q) \end{cases}, \quad \Theta_{M,i} = \begin{cases} 1, & \mu_{Bkg}(i) > \mu_{Obj}(i) \\ \Theta_i, & \mu_{Bkg}(i) \leq \mu_{Obj}(i) \end{cases},$ $\mu_{Bkg}(i) = 1 - \mu_{Obj}(i), \quad \mu_{Obj}(i) = \exp\left(-\frac{(x_i - x_m)^2}{2\sigma_x^2}\right) \exp\left(-\frac{(y_i - y_m)^2}{2\sigma_y^2}\right).$ The variables of each equation are described in Section 3.1.
Fault Tolerance to seeds localization	Low	High

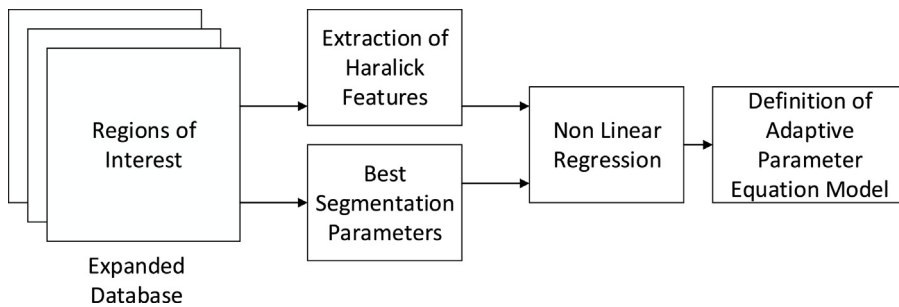


Fig. 4. Flowchart of the definition of the adaptive parameter equation model. This process was performed only once to define the parameter equation.

knowledge. Our proposed modified evolution rule differs from original GrowCut because in GrowCut it depends only on the strength of the attacking cell and difference of intensity values, while in the proposed method it also consider a fuzzy membership function. As the region of tumor is uncertain, it is more adequate to use a fuzzy membership function to guide the update of cells, where regions with higher value of the membership function related to background will have a different value of strength compared to the lower ones. This modification makes the algorithm less susceptible to segment areas outside the region of interest.

3.2. Automatic selection of seeds

The selection of seeds consists of identifying initial pixels located in regions of tumor and non-tumor. In many seed-based techniques, such as Random Walks [33] and Graph Cut [34], seeds are selected manually by a specialist. An important characteristic of the proposed algorithm is that it is not necessary to select non-tumor seeds, because the proposed algorithm can adjust its Gaussian Fuzzy frontier based only on the seeds of the tumor region.

In this work, we used the Differential Evolution optimization algorithm [35] to find automatically seeds in the region of the object of interest, i.e. the suspicious lesion. The solution is represented as a set of seeds, which explore the coordinates of image to find the best representations of initial seeds. The number of seeds per solution is an algorithm parameter which is configured in the adaptive step of the proposed method. Knowing that mass regions frequently have higher intensity pixel values, the problem of finding an adequate set of seeds was converted into an optimization problem, in which we are interested in finding a set of points with maximum distance between each one, and maximum sum of associated gray levels, in order to obtain a non-collapsing set of points located inside the brighter areas. For this purpose, we used a multi-objective fitness function, which evaluates both the distance between seed points and the levels of intensity of the pixels related to them.

3.3. Adaptive selection of parameters

The semi-supervised GrowCut modification requires two parameters configuration: the number of points represented by a solution in the Differential Evolution algorithm and the α value from the Fuzzy membership degree, described in Eq. (5). However, the best configuration parameters can vary according to the selected region of interest, as most of segmentation algorithms described in Section 2. The problem is that the selection of parameters still requires a specialist knowledge, which is dependent on professional experience and susceptible to human failure. Although the segmentation method is automatic, the selection of parameters still requires a configuration by a specialist. On the other hand, the process of selection of parameters can be automatized from the definition of an equation that maps the characteristics of the chosen region of interest and the best parameters of the modified GrowCut.

Table 2
Haralick features used for feature extraction.

Number	Feature
1	Energy
2	Contrast
3	Correlation
4	Sum of variance
5	Inverse difference moment
6	Sum average
7	Sum variance
8	Sum entropy
9	Entropy
10	Difference variance
11	Difference entropy
12	Info. measure of correlation 1
13	Info. measure of correlation 2

The adaptive parameter equation consists of suggesting a configuration to the Fuzzy GrowCut algorithm, based on the features of the ROI. Nevertheless, this equation is not known and therefore we assume that it can be approximated by a quadratic equation, using the method of linear regression. To obtain the definition of the adaptive parameter equation model, initially it was performed an exhaustive search in the Fuzzy GrowCut configuration space to find the best segmentation parameters for each ROI of the database. Next, we applied a non linear regression based on the ROIs features and the best segmentation parameters for each ROI. The results of non linear regression provides the definition adaptive parameter model. This process was performed only once to define the parameter equation. This flow is shown in Fig. 4.

To perform the regression, firstly, we performed an expansion of the database. The expansion consisted in adding Gaussian noise to the original database, creating a set of 171 ROIs. Next, were extracted the The Haralick features [36], which have been successful applied to classify masses in mammograms [37]. The Haralick features consists of 13 descriptors, which are described in Table 2.

Once the best parameters for each ROI were identified, the 13 Haralick features were used as input parameters for the non linear regression model, while the best segmentation parameters were used as desired output to the regression. The equation is approximated by a quadratic model function, which is represented by the Eq. (7):

$$f(x_1, x_2, \dots, x_{13}) = w_0 + \sum_{i=1}^{13} w_i \cdot x_i + \sum_{i=1}^{13} \sum_{k=1}^{13} w_{13i+k} \cdot x_i \cdot x_k, \quad (7)$$

where x_1, x_2, \dots, x_{13} represents the 13 Haralick features and w_i is the weight of the function. The equation is composed by 105 weights, whose values are provided as the results of the regression. The adaptive parameter equation maps the relation between the Haralick features and the best configurations of the algorithm. Therefore, once estimated the weights of the equation, it is necessary only to provide the Haralick features of an ROI to obtain the

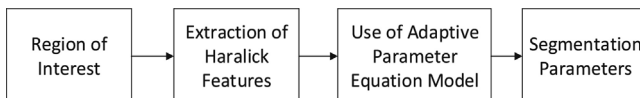


Fig. 5. Automatic configuration of segmentation parameters.

prediction of best parameters of the algorithm. **Fig. 5** shows the process of automatic configuration of segmentation parameters, which is used for each ROI of the database.

This turns the method adaptive because we defined an equation, with weights estimated through non linear regression, that provides the segmentation parameters of the proposed algorithm based on the features of each region of interest.

3.4. Methodology

The flowchart of **Fig. 6** illustrates the methodology we are proposing. The proposed approach is called semi-supervised because it has a supervised and an unsupervised step, as described in **6**. Firstly, in the supervised step, a specialist selects the region of interest, generating a sub-image as input for the segmentation

method. Afterwards, in the unsupervised step, the Haralick Features are extracted and applied to the Eq. (7), which will provide the algorithm parameters to the ROI. Next, the Differential Evolution optimization algorithm automatically selects points internal to the probable mammary lesion. These seed points are located by an optimization process guided by a multi-objective fitness function to maximize the distance between points and the brightness of the pixels' positions. Subsequently, our modified GrowCut algorithm performs the segmentation, generating a labeled image. Hence, once given a region of interest, segmentation is performed automatically. **Fig. 7** illustrates the steps of the proposed method for some images of the MiniMIAS database.

Column *a* of **Fig. 7** represents the initial region of interest, manually selected from the MiniMIAS database. Column *b* shows the seed points obtained from automatic seeds selection. As cited in the previous section, the proposed technique requires only seeds of the tumor region. Column *c* illustrates the boundaries of the Gaussian fuzzy region, where the inside region has higher membership degrees of pixels internal to the lesion mass. The size of the Gaussian region is based on the location of seed points. Column *d* shows the final segmentation of the proposed method, while the column *e* shows the ground truth of the image. Finally, column *f* shows the

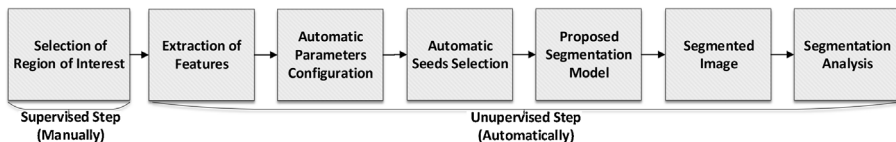


Fig. 6. Flowchart of the proposed methodology.

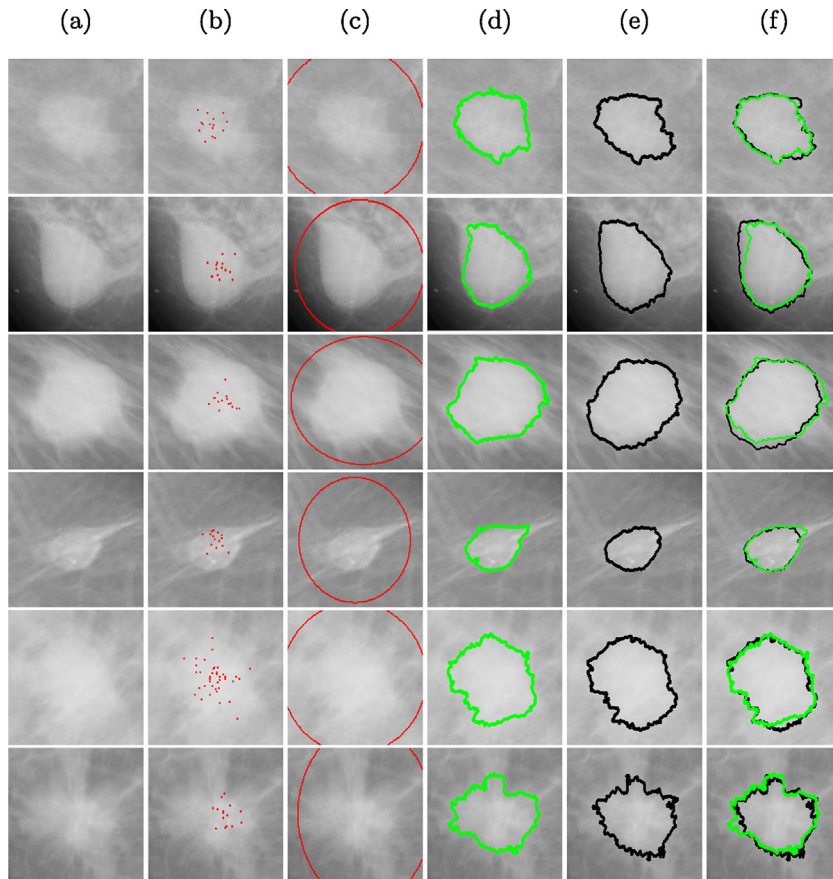


Fig. 7. Images mdb010, mdb021, mdb028, mdb132, mdb063, and mdb181, obtained from MiniMIAS database, illustrating the proposed semi-supervised segmentation method. (a) Original image; (b) automatic generated seeds; (c) Gaussian fuzzy region; (d) segmentation of Fuzzy GrowCut; (e) ground truth (f) and final segmentation (green) compared to ground truth image (black). (For interpretation of the references to color in this figure legend, the reader is referred to the web version of the article.)

final segmentation of the proposed approach, in green, compared with the ground-truth contour, in black.

3.5. Experimental environment

In order to validate our segmentation method, we used 57 images from the Mammographic Image Analysis Mini-Mammographic Database (MiniMIAS) [38]. This database contains a total of 322 Mediolateral-Oblique (MLO) mammogram view images, of which only 59 contains lesions, subdivided as spiculated, circumscribed and ill-defined margin types. MiniMIAS images are 200 μ m pixel edge with resolution of 1024 × 1024 pixels. Two images of lesion were discarded because the dataset did not provide the indication of tumor regions. Therefore we selected 57 images: 25 circumscribed, 19 spiculated, and 15 ill-defined lesions. Ground-truth images were generated by using a pre-built supervised auxiliary software, based on adaptive threshold and specialist knowledge. For the generation of the adaptive parameter equation model, we expanded the database using Gaussian noise, creating a set of 171 ROIs. For segmentation analysis, the original 57 images were used.

3.6. Metrics

Results were evaluated using 9 metrics. To evaluate the accuracy of shape between the segmented region and ground-truth, the following metrics were used: Area, Perimeter, Form Factor, Solidity, Feret's Distance, and Area Overlap Measure (AOM). Those metrics were chosen because they provide information about the shape of the segmentation, which is a more complete evaluation of the quality and shape of the segmentation, instead of only using the AOM measure. To evaluate true and false positives, we used Sensitivity, Specificity, and Balanced Accuracy.

The Area corresponds to the number of pixels in the region occupied by the object of interest, i.e. the suspicious lesion. It is expected that segmented images and ground-truth images have approximately the same numerical areas.

The Perimeter (Per) is the distance, in pixels, around the boundary of the region. Although regions with different shapes can have the same perimeter, when combined with other metrics, it is important to evaluate the similarity of regions.

The Form Factor furnishes a comparison between the area of a polygon with the square of its perimeter. In a circle, the Form Factor is 1, whilst we have $\pi/4$ for a square. This metric is defined by the expression of Eq. (8):

$$\text{FormFactor} = \frac{4\pi \text{Area}}{\text{Perimeter}^2}. \quad (8)$$

Solidity is a measure of the intersection between the proper area and the convex area, given by the expression of Eq. (9):

$$\text{Solidity} = \frac{\text{Area}}{\text{ConvexArea}}. \quad (9)$$

The solidity value of a convex polygon, with no holes, is equal to 1.0, representing a solid object. When solidity is lower than 1.0, the object is considered irregular or contains a hole. Hence, solidity helps to indicate the shape of the object.

Feret's diameter is the longest distance between any two points along the selection boundary, also known as maximum caliper. In this work, the angle of Feret's diameter is calculated for 0 and 90 degrees, which represents the maximum distance in coordinates x and y , named as FeretX (FX) and FeretY (FY). It is important to note that the metrics related to shape should be analyzed together and not individually.

For each metric, an error measure is defined, based on the metric applied to the segmented image and the ground-truth result. The error of each metric is defined by Eq. (10), as follows:

$$E_{\text{Metric}} = 1 - \exp \left(- \frac{|\text{Metric}_{\text{Seg}} - \text{Metric}_{\text{GT}}|}{\text{Metric}_{\text{GT}}} \right), \quad (10)$$

where $\text{Metric}_{\text{Seg}}$ and $\text{Metric}_{\text{GT}}$ are the metric values for the segmented and ground-truth images, respectively.

The Area Overlap Measure (AOM) is one of the most used metric in state-of-the-art to measure the quality of tumor segmentation. The AOM shows the overlap area between segmented image and ground-truth. The AOM is defined by Eq. (11):

$$\text{AOM} = \frac{\text{Area}(\text{Seg} \cap \text{GT})}{\text{Area}(\text{Seg} \cup \text{GT})}, \quad (11)$$

where Seg represents the segmented image and GT the ground-truth.

Sensitivity measures the true positivity recognition rate. In this work, sensitivity is evaluated for the classification of pixels, being described as follows:

$$\text{Sensitivity} = \frac{|\text{F}_{\text{Seg}} \cap \text{F}_{\text{GT}}|}{|\text{F}_{\text{Seg}} \cap \text{F}_{\text{GT}}| + |\text{B}_{\text{Seg}} \cap \text{B}_{\text{GT}}|}, \quad (12)$$

where F_{Seg} and F_{GT} are the number of foreground pixels of the segmentation and ground-truth, respectively, whilst B_{Seg} and B_{GT} are the number of background pixels of segmentation and ground-truth, in this order.

Specificity measures the true negative recognition rate. It is described as following:

$$\text{Specificity} = \frac{|\text{B}_{\text{Seg}} \cap \text{B}_{\text{GT}}|}{|\text{B}_{\text{Seg}} \cap \text{B}_{\text{GT}}| + |\text{F}_{\text{Seg}} \cap \text{B}_{\text{GT}}|}. \quad (13)$$

Having a high sensitivity and low specificity does not necessarily mean good segmentation. Therefore, the Balanced Accuracy is defined as the average of Sensitivity and Specificity, describing both the negative and positive recognition rates, as following:

$$\text{BAC} = \frac{\text{Sensitivity} + \text{Specificity}}{2} \quad (14)$$

4. Results

This section describes the main results obtained when using the proposed Fuzzy GrowCut, comparing the segmentation results with state-of-art techniques. First, we analyzed how fault tolerant is our approach when compared with classical GrowCut. This analysis is done in the next subsection.

4.1. Fault Tolerance Analysis

The original GrowCut, as the most of seed based techniques, is very sensitive about the localization of the initial seeds. Usually, a wrong seed selection by a specialist can determine the quality of segmentation. This is not desired in a supervised method, once the supervised step is subject to human failure. For this analysis, we compared the segmentation with the seeds labeled correctly and with a variation of a seed, positioning it wrongly. Fig. 9 shows how the localization of seed points in GrowCut influences in the final segmentation.

In Fig. 9, column *a* shows the original ROI, column *b* and *c* shows seeds placed correctly and segmentation obtained, respectively. The points in red are seeds labeled as tumor class and the blue ones as the non-tumor class. Column *d* shows the seeds selected, but with an seed of tumor label misplaced outside the region of tumor.

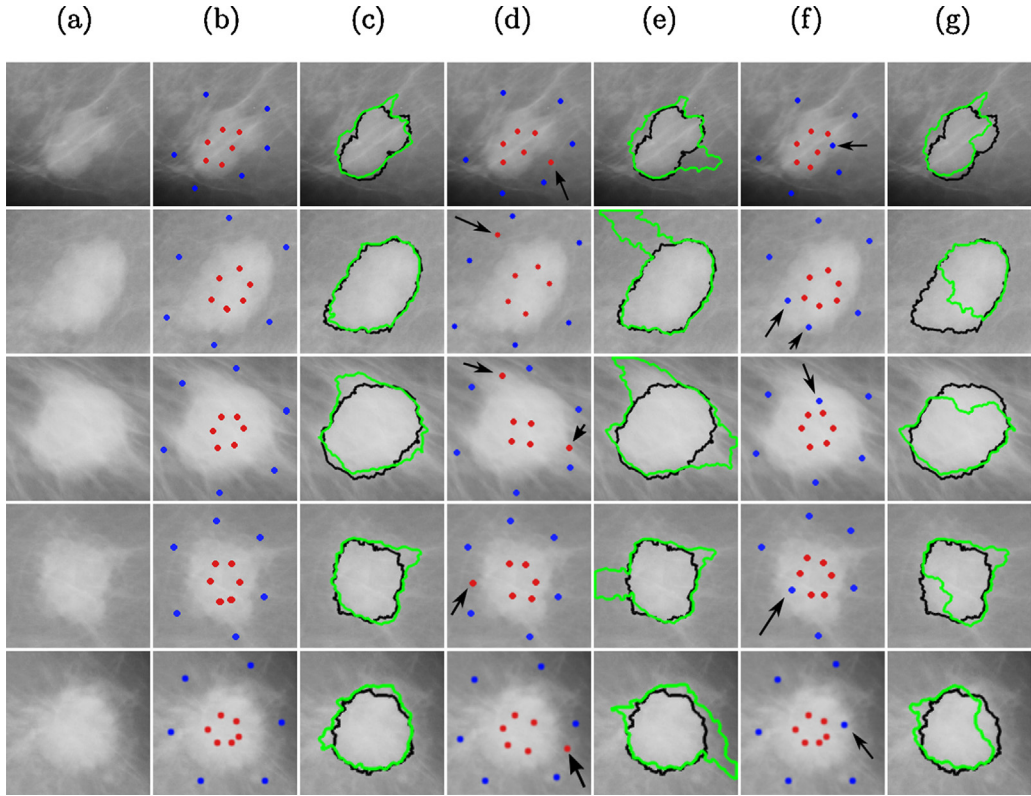


Fig. 8. Fault Tolerance Analysis of the seed points of GrowCut.

The black arrow in each figure shows the seed that is wrongly positioned. Column e shows the segmentation obtained with the seeds from column d. Column f shows the seed selection, but with a seed of non-tumor label positioned at a wrong location, which is indicated by the black arrow. Finally, column g shows the segmentation obtained from the seeds of column f.

From Fig. 9 we can observe that a wrong seed selection can result in an inaccurate segmentation. Therefore, the GrowCut cannot be considered to be fault tolerant related to seeds selection. In the proposed Adaptive Fuzzy GrowCut, we removed the need selection of non-tumor seeds, and the algorithm is based on the center of mass and standard deviation of tumor seeds, which reduces the sensibility of the algorithm and improve its Fault Tolerance. Fig. 8 shows the analysis of seeds location and segmentation performed to the proposed method.

Column a from Fig. 8 shows the original ROI, column b shows the seeds selected by the user and the Gaussian region generated through the proposed method, and column c shows the segmentation obtained using the seeds shown in column b. Column d shows the seed points with a wrongly positioned seed, indicated by the black arrow. Column e shows the segmentation obtained using seeds from column d. The ROIs used in this analysis are the same used in Fig. 9 and can be verified from Fig. 8 that the Fuzzy GrowCut is more fault tolerant to small variations of seed points, as can be observed comparing columns c and e, as the segmentation had small variations.

Results from Figs. 8 and 9 shows that the proposed method has an improvement, compared to the original GrowCut, because it is more fault tolerant in relation to the selection of seeds. As the step of seeds selection in original GrowCut is a supervised process, it is susceptible to human errors, and a misplaced seed can result in an inaccurate segmentation. The proposed modified GrowCut, besides turning the selection of seeds an unsupervised process, it is robust in terms of seeds positioning. Although we adopted an

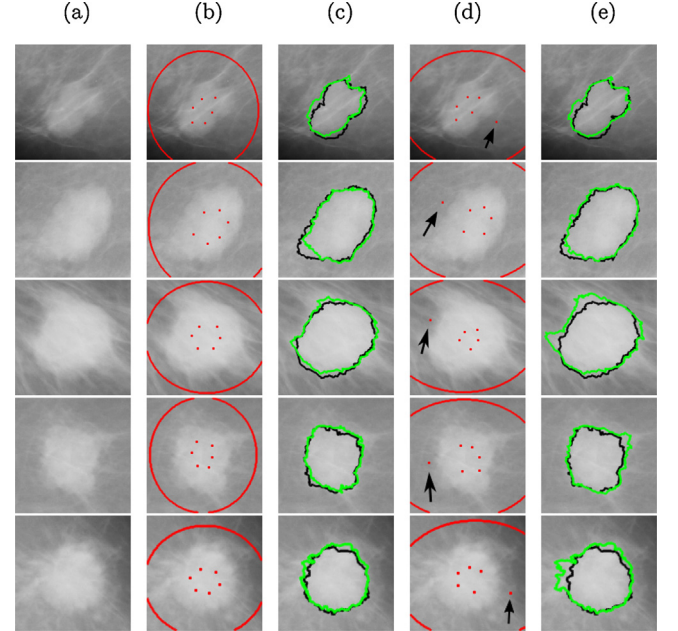


Fig. 9. Fault Tolerance of the seed points of Fuzzy GrowCut.

unsupervised selection of seeds, this process can be replaced by a supervised selection, if desired.

4.2. General results

The results were analyzed for all images with lesions from MiniMIAS, corresponding to 57 images divided into circumscribed, spiculated and those with ill-defined margins. Six state-of-the-art

Table 3

Best parameters of BEMD, MCW and topographic techniques.

Technique	Best parameters
BEMD	$r_i = 0.4$
MCW	$\text{size}_{se} = 7$; $\text{type}_{se} = \text{square}$
Topographic	$n_{levels} = 10$; $depth = 2$

works were compared to the proposed technique: BEMD [30], BMCS [39], LBI [40], MCW [20], Topographic Approach [22], and Wavelet Analysis [29].

We performed an optimization of the parameters of each technique through an exhaustive search. The best parameters found for techniques BEMD, MCW and Topographic Approach are described in Table 3. The BMCS, LBI and Wavelet Analysis do not have parameters.

The results of the segmentation of each technique were evaluated through the metrics described in the previous section. Fig. 10 shows the results of segmentation of all techniques analyzed for the images mdb010, mdb021, mdb028, mdb190, mdb132, and mdb312.

The first column of Fig. 10, from left to right, presents the initial regions of interest, while the following columns are the segmentation results of the following techniques: Topographic Approach, Wavelet, BEMD, BMCS, LBI, and MCW, in this order. Ground-truth contours are represented in black, while the borders of segmentation results are presented in green. The modified Grow-Cut and the Topographic technique obtained contours very close

to ground-truths for all images of Fig. 10, whilst other techniques had more difficulties with images mdb312 and mdb021. However, the proposed approach get better segmentation results than the topographic technique for images mdb010 and mdb021. Although Fig. 10 shows only six examples, the analysis was performed on all images. The average values of the metrics for each technique are shown in Table 4.

In Table 4, bold numbers represent the best values for each metric. The error values of area, form factor, perimeter, Ferret Distance related to axis X, Ferret Distance related to axis Y, and solidity are represented as E_{Area} , $E_{\text{FormFactor}}$, E_{Per} , E_{FX} , E_{FY} , and E_{Solidity} , respectively. For these metrics, the lowest values are associated to the best results. Area Overlap Measure and Balanced Accuracy metrics are represented as AOM and BAC, respectively. For Sensitivity, Specificity and BAC, the higher the measures, the better the segmentation. The proposed segmentation method obtained the lowest error values and the highest AOM.

From Table 4, we can observe that the proposed technique had lower error values for most of metrics. This indicates that the obtained segmentation had a shape closer to the ground-truth images, on average. The metric BMCS had a high sensitivity, but a low specificity. That means that most of the pixels were classified as tumor, resulting in many false positives. The Topographic Approach had a higher specificity, which means a high true negative rate, but the proposed technique had a higher balanced accuracy, which is the mean between Sensitivity and Specificity. Boxplots of all metrics for these results are illustrated in Figs. 11 and 12.

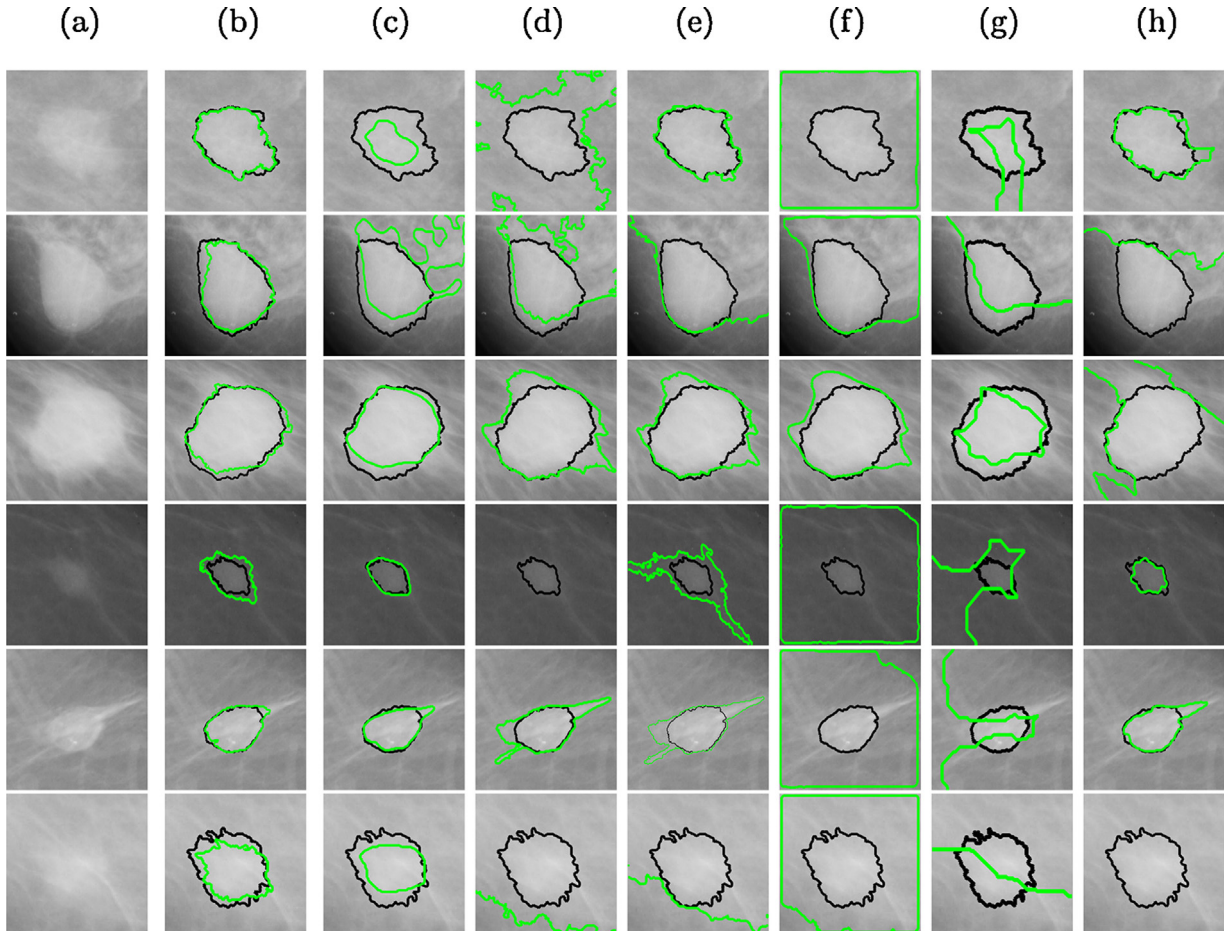


Fig. 10. Comparison of segmentation results with state-of-the-art techniques, for MiniMIAS images mdb010, mdb021, mdb028, mdb190, mdb132, and mdb312. (a) Region of interest; (b) proposed method; (c) topographic; (d) wavelet; (e) BEMD; (f) BMCS; (g) LBI; (h) MCW.

Table 4

Average values of the metrics for the techniques analyzed, for all types of lesion.

Metrics	BEMD	BMCS	LBI	MCW	Proposed	Topographic	Wavelet
E_{Area}	0.72 ± 0.29	0.77 ± 0.29	0.48 ± 0.30	0.48 ± 0.36	0.34 ± 0.31	0.37 ± 0.26	0.60 ± 0.29
$E_{\text{FormFactor}}$	0.40 ± 0.27	0.44 ± 0.29	0.37 ± 0.24	0.33 ± 0.24	0.26 ± 0.25	0.45 ± 0.27	0.36 ± 0.20
E_{Per}	0.63 ± 0.29	0.43 ± 0.26	0.31 ± 0.20	0.35 ± 0.24	0.27 ± 0.25	0.33 ± 0.23	0.53 ± 0.27
E_{FX}	0.47 ± 0.27	0.44 ± 0.26	0.31 ± 0.22	0.31 ± 0.22	0.20 ± 0.21	0.24 ± 0.18	0.37 ± 0.23
E_{FY}	0.47 ± 0.27	0.44 ± 0.26	0.29 ± 0.23	0.30 ± 0.21	0.20 ± 0.21	0.26 ± 0.23	0.37 ± 0.22
E_{Solidity}	0.18 ± 0.25	0.11 ± 0.10	0.13 ± 0.11	0.11 ± 0.12	0.09 ± 0.15	0.11 ± 0.15	0.14 ± 0.13
AOM	0.38 ± 0.24	0.35 ± 0.24	0.31 ± 0.20	0.43 ± 0.24	0.58 ± 0.24	0.51 ± 0.22	0.42 ± 0.25
Sensitivity	0.91 ± 0.26	0.98 ± 0.05	0.52 ± 0.20	0.75 ± 0.26	0.82 ± 0.22	0.70 ± 0.22	0.83 ± 0.31
Specificity	0.59 ± 0.22	0.39 ± 0.27	0.78 ± 0.17	0.66 ± 0.35	0.84 ± 0.18	0.88 ± 0.14	0.64 ± 0.34
BAC	0.75 ± 0.12	0.69 ± 0.13	0.65 ± 0.13	0.71 ± 0.16	0.83 ± 0.13	0.79 ± 0.11	0.73 ± 0.16

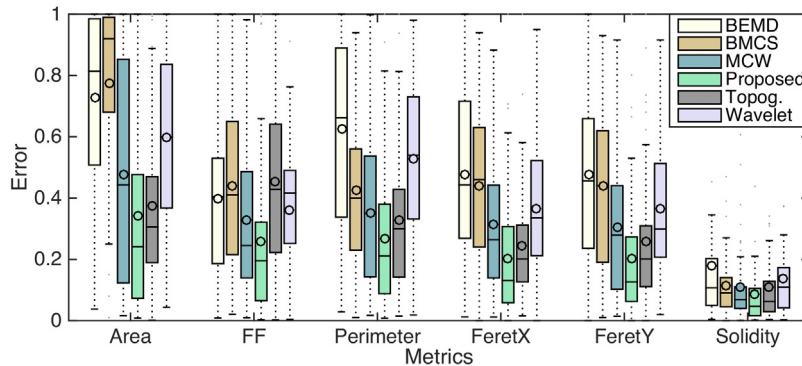


Fig. 11. Average values of the metrics for the state-of-the-art techniques, in comparison with our proposed method, for all types of lesion.

From Figs. 11 and 12 we can perceive that the proposed technique achieved the lowest average error, with lower median and lower range, for most of the metrics based on errors. Regarding AOM, Sensitivity, Specificity, and BAC, the proposed segmentation method reached a position among the techniques with best performances, achieving the best values for AOM and Specificity.

In order to differentiate our proposal from other state-of-the-art methods, we employed the Wilcoxon Signed Rank Test [41], considering as null hypothesis the equality of two means, using a confidence level of 95%. Results are shown in Table 5.

From Table 5, values below 0.05 are interpreted as rejection of the null hypothesis, i.e. populations under test are equal, with a confidence level of 95%. Consequently, Table 5 shows that the proposed segmentation algorithm achieved the statistically best results for all metrics when compared to Wavelet, BEMD, BMCS and MCW techniques. When compared to Topographic Approach the results were similar the metrics of Form Factor Ferret X and Solidity. However, for most of the metrics the results were statistically better, as shown in Table 4. Despite the results from Table 5,

these results should be analyzed together, since an isolated good result for one of these two metrics is not necessarily associated to good segmentation performance. Besides, the proposed technique has the advantage of having no parameters when compared with Topographic Approach.

We also analyzed the metrics of the segmented images for each type of tumor, separately, in order to identify which technique is most suitable for each type of mammary lesion. Table 6 presents the average results for circumscribed lesions images.

From Table 6 we can perceive that the modified GrowCut, MCW, Topographic Approach, and Wavelet are among the techniques achieving the lowest errors for circumscribed mammary lesions. From the boxplots of Fig. 13 and 14 we can also notice that the proposed segmentation method achieved results with small standard deviations as well, for most metrics. Average results of metrics for spiculated lesions images are shown on Table 7.

From Table 7 we can notice that the proposed approach obtained the best results for all metrics, demonstrating that the semi-supervised modified GrowCut algorithm is more suitable to

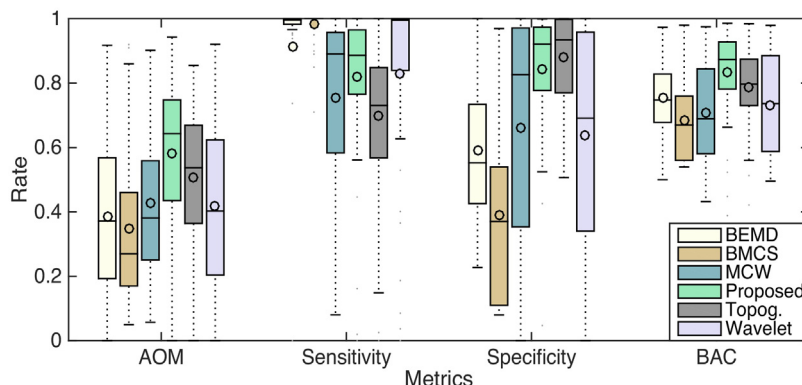


Fig. 12. Average values of the metrics for the state-of-the-art techniques, in comparison with our proposed method, for all types of lesion.

Table 5

P-value of Wilcoxon Signed Rank Test comparing the proposed approach with the analyzed techniques.

Comparison	E_{Area}	$E_{\text{FormFactor}}$	E_{Per}	E_{FX}	E_{FY}	E_{Solidity}	AOM	BAC
Topographic	1.37e-01	5.91e-05	4.97e-02	2.86e-02	6.29e-02	8.33e-02	5.16e-03	3.59e-03
Wavelet	1.69e-05	5.76e-03	1.95e-07	1.88e-05	5.82e-06	3.24e-03	6.32e-05	5.73e-04
BEMD	1.94e-09	2.57e-04	1.85e-09	5.37e-08	2.99e-08	5.09e-04	2.99e-06	8.82e-05
BMCS	1.89e-09	8.53e-05	4.64e-06	2.57e-07	1.83e-07	9.90e-04	2.99e-06	5.40e-06
MCW	2.28e-02	6.47e-02	4.08e-03	3.64e-04	7.97e-04	1.63e-01	4.91e-05	2.61e-06

Table 6

Average values of the metrics for the techniques analyzed, for circumscribed lesions.

Metrics	BEMD	BMCS	LBI	MCW	Proposed	Topographic	Wavelet
E_{Area}	0.67 ± 0.31	0.71 ± 0.32	0.45 ± 0.29	0.41 ± 0.35	0.38 ± 0.36	0.41 ± 0.27	0.46 ± 0.27
$E_{\text{FormFactor}}$	0.40 ± 0.30	0.37 ± 0.28	0.34 ± 0.26	0.24 ± 0.23	0.30 ± 0.30	0.37 ± 0.25	0.39 ± 0.18
E_{Per}	0.60 ± 0.30	0.41 ± 0.24	0.32 ± 0.20	0.31 ± 0.22	0.33 ± 0.31	0.30 ± 0.21	0.45 ± 0.30
E_{FX}	0.45 ± 0.30	0.40 ± 0.26	0.28 ± 0.22	0.26 ± 0.20	0.25 ± 0.28	0.26 ± 0.17	0.28 ± 0.18
E_{FY}	0.44 ± 0.28	0.39 ± 0.26	0.30 ± 0.27	0.24 ± 0.17	0.23 ± 0.28	0.25 ± 0.20	0.28 ± 0.18
E_{Solidity}	0.19 ± 0.27	0.08 ± 0.07	0.13 ± 0.12	0.08 ± 0.07	0.15 ± 0.23	0.06 ± 0.06	0.13 ± 0.10
AOM	0.43 ± 0.26	0.40 ± 0.25	0.34 ± 0.23	0.51 ± 0.26	0.53 ± 0.29	0.48 ± 0.21	0.49 ± 0.25
Sensitivity	0.90 ± 0.29	0.98 ± 0.04	0.53 ± 0.22	0.77 ± 0.25	0.77 ± 0.30	0.70 ± 0.22	0.76 ± 0.32
Specificity	0.62 ± 0.24	0.44 ± 0.27	0.78 ± 0.18	0.74 ± 0.31	0.86 ± 0.14	0.85 ± 0.16	0.79 ± 0.25
BAC	0.76 ± 0.13	0.71 ± 0.13	0.66 ± 0.14	0.75 ± 0.16	0.81 ± 0.17	0.78 ± 0.11	0.78 ± 0.14

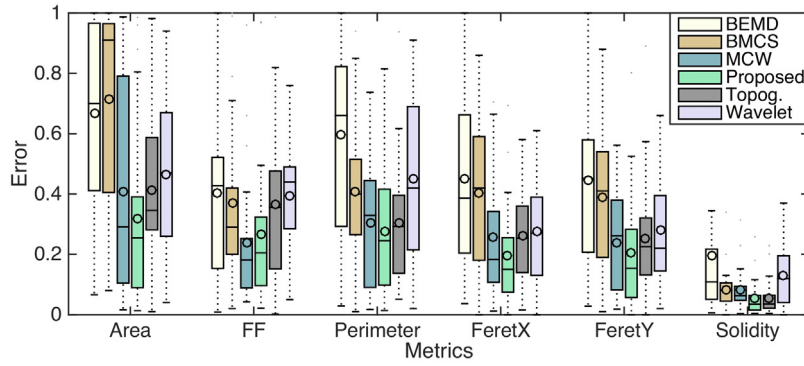


Fig. 13. Average values of the metrics for the state-of-the-art techniques and the proposed semi-supervised GrowCut, for circumscribed lesions images.

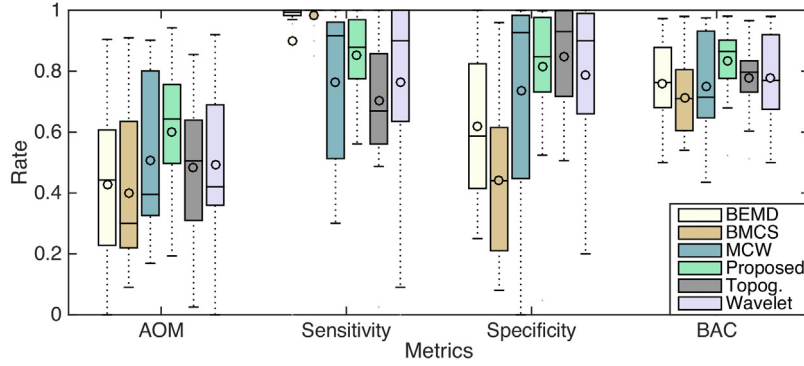


Fig. 14. Average values of the metrics for the state-of-the-art techniques and the proposed semi-supervised GrowCut, for circumscribed lesions images.

Table 7

Average values of the metrics for the techniques analyzed, for spiculated lesions.

Metrics	BEMD	BMCS	LBI	MCW	Proposed	Topographic	Wavelet
E_{Area}	0.83 ± 0.23	0.84 ± 0.23	0.54 ± 0.35	0.58 ± 0.37	0.38 ± 0.36	0.45 ± 0.27	0.72 ± 0.25
$E_{\text{FormFactor}}$	0.46 ± 0.24	0.44 ± 0.32	0.44 ± 0.27	0.47 ± 0.25	0.30 ± 0.30	0.53 ± 0.30	0.38 ± 0.22
E_{Per}	0.71 ± 0.27	0.51 ± 0.27	0.35 ± 0.24	0.48 ± 0.24	0.33 ± 0.31	0.40 ± 0.30	0.64 ± 0.23
E_{FX}	0.55 ± 0.27	0.51 ± 0.26	0.37 ± 0.23	0.42 ± 0.23	0.25 ± 0.28	0.29 ± 0.23	0.47 ± 0.24
E_{FY}	0.53 ± 0.28	0.50 ± 0.27	0.37 ± 0.22	0.39 ± 0.26	0.23 ± 0.28	0.33 ± 0.29	0.46 ± 0.26
E_{Solidity}	0.20 ± 0.22	0.14 ± 0.12	0.14 ± 0.10	0.16 ± 0.15	0.15 ± 0.23	0.17 ± 0.22	0.18 ± 0.18
AOM	0.30 ± 0.21	0.29 ± 0.21	0.26 ± 0.18	0.30 ± 0.19	0.53 ± 0.29	0.45 ± 0.23	0.32 ± 0.22
Sensitivity	0.92 ± 0.23	0.98 ± 0.07	0.53 ± 0.22	0.71 ± 0.29	0.77 ± 0.30	0.69 ± 0.27	0.83 ± 0.33
Specificity	0.54 ± 0.20	0.37 ± 0.25	0.77 ± 0.14	0.55 ± 0.39	0.86 ± 0.14	0.87 ± 0.13	0.56 ± 0.34
BAC	0.73 ± 0.11	0.67 ± 0.12	0.65 ± 0.13	0.63 ± 0.15	0.81 ± 0.17	0.78 ± 0.14	0.69 ± 0.15

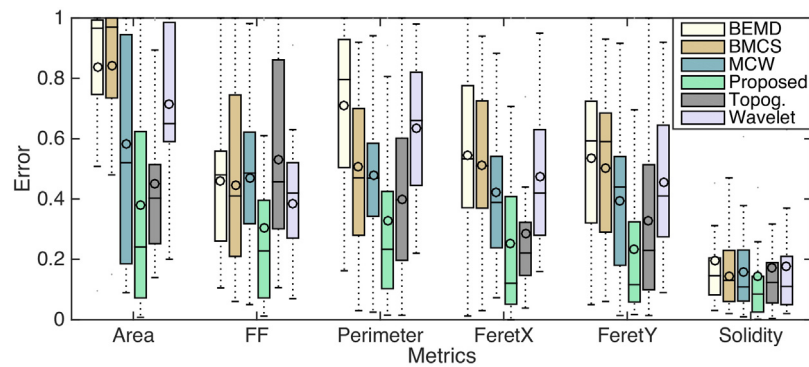


Fig. 15. Average values of the metrics for the state-of-the-art techniques and the proposed semi-supervised GrowCut, for spiculated lesions images.

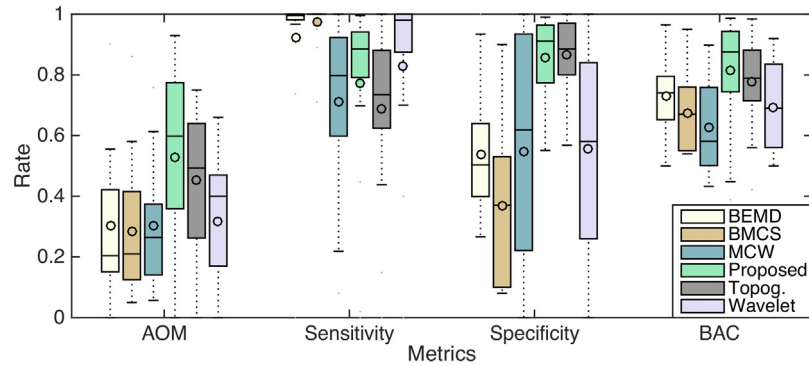


Fig. 16. Average values of the metrics for the state-of-the-art techniques and the proposed semi-supervised GrowCut, for spiculated lesions images.

segment spiculated lesion images. Borders of spiculated lesions are usually hard to segment, due to their irregular edges. The high specificity indicates a high false positive rate, which provided a good balanced accuracy. Boxplots of all metrics for spiculated images are provided in Figs. 15 and 16.

Based on Figs. 15 and 16, we can perceive that the proposed method assumed the lowest average error values, with the lowest standard deviations as well. For metrics AOM and BAC, the proposed technique was equivalent to the other state-of-the-art approaches. Average results of metrics for indistinct type of masses are shown in Table 8.

From Table 8 we can notice that the proposed semi-supervised Fuzzy GrowCut could achieve the lowest errors for Form Factor, Feret's Distance, Solidity, and AOM. For the other metrics, the proposed method demonstrated equivalence to the other techniques, with close results. This indicates that the proposed technique is also suitable for ill-defined lesions, with some characteristics of shape more close to the ground-truth, as indicated by Form Factor and Solidity metrics. Results for Balanced Accuracy achieved the higher result, demonstrating the high average value between Sensitivity

and Specificity. Boxplots of all metrics for indistinct types of tumor are illustrated in Figs. 17 and 18.

The proposed approach was compared to 6 state-of-the-art techniques, demonstrating its suitability to segment masses of mammograms of MiniMIAS image database. Although results could be considered accurate for all types of mammary lesions, considering all shape metrics used in this work, results of segmentation indicated that the proposed technique can obtain a better quality of segmentation for spiculated and ill-defined lesions, when compared to state-of-the-art techniques. These types of lesion usually are harder to segment using automatic methods. Although for some metrics, the Fuzzy GrowCut had statistically similar quality of segmentation when compared to Topographic Approach, the Adaptive Fuzzy GrowCut has the advantage of having no parameters to be adjusted.

5. Discussion

The results presented compared the proposed approach with state-of-the-art techniques through a qualitative and quantitative

Table 8

Average values of the metrics for the techniques analyzed, for ill-defined lesions.

Metrics	BEMD	BMCS	LBI	MCW	Proposed	Topographic	Wavelet
E_{Area}	0.69 ± 0.31	0.78 ± 0.31	0.46 ± 0.26	0.45 ± 0.35	0.32 ± 0.25	0.23 ± 0.16	0.66 ± 0.28
$E_{\text{FormFactor}}$	0.32 ± 0.24	0.53 ± 0.23	0.34 ± 0.17	0.29 ± 0.14	0.19 ± 0.18	0.49 ± 0.24	0.28 ± 0.17
E_{Per}	0.57 ± 0.31	0.35 ± 0.25	0.25 ± 0.16	0.25 ± 0.19	0.17 ± 0.16	0.28 ± 0.15	0.51 ± 0.23
E_{FX}	0.42 ± 0.30	0.40 ± 0.27	0.26 ± 0.21	0.25 ± 0.21	0.15 ± 0.11	0.16 ± 0.10	0.36 ± 0.25
E_{FY}	0.45 ± 0.26	0.43 ± 0.24	0.19 ± 0.15	0.28 ± 0.18	0.16 ± 0.13	0.17 ± 0.14	0.38 ± 0.20
E_{Solidity}	0.13 ± 0.25	0.12 ± 0.10	0.10 ± 0.08	0.08 ± 0.12	0.07 ± 0.06	0.11 ± 0.10	0.09 ± 0.05
AOM	0.42 ± 0.26	0.35 ± 0.25	0.31 ± 0.18	0.47 ± 0.22	0.62 ± 0.20	0.61 ± 0.19	0.42 ± 0.25
Sensitivity	0.92 ± 0.26	0.99 ± 0.02	0.48 ± 0.15	0.79 ± 0.25	0.83 ± 0.21	0.70 ± 0.17	0.93 ± 0.25
Specificity	0.62 ± 0.22	0.33 ± 0.31	0.81 ± 0.18	0.70 ± 0.33	0.88 ± 0.17	0.95 ± 0.08	0.50 ± 0.38
BAC	0.77 ± 0.12	0.66 ± 0.15	0.64 ± 0.11	0.74 ± 0.14	0.86 ± 0.11	0.82 ± 0.09	0.72 ± 0.19

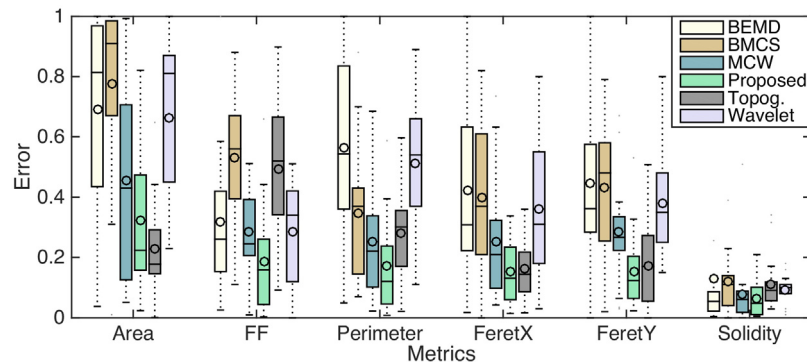


Fig. 17. Boxplot of the average values of the metrics for the techniques analyzed, for ill-defined lesions.

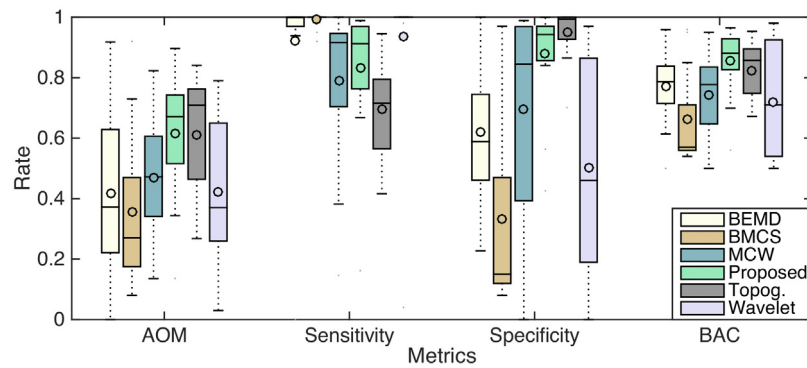


Fig. 18. Boxplot of the average values of the metrics for the techniques analyzed, for ill-defined lesions.

analysis. The qualitative analysis indicates that the Fuzzy GrowCut can obtain good segmentation when compared to state-of-art techniques, having the advantage of requiring no parameters to be tuned. Although the improvement of segmentation techniques in the literature, it can be observed that the segmentation techniques still have difficulties in achieving an accurate segmentation of tumors, specially for spiculated and ill-defined lesions. This work contributes improving the quality of semi-supervised segmentation for these scenarios, however, enhancements still are required to segmentation get closer to the ground truth.

Quantitative results showed that the proposed approach achieved better results, specially to spiculated and ill-defined lesions, when compared to state-of-the-art techniques. One point of discussion is why no technique was better for all metrics analyzed. The fact is that each technique evaluates a different aspect of the shape of segmentation. The BMCS, for example, had high values of sensitivity for all types of tumor because it had over segmentation for most of cases, while having a low specificity. Usually, a good segmentation have high values for both sensitivity and specificity, which is evaluated by the metric BAC. The metric of area, for example, in Table 8, has lower value for the Topographic Approach. This means that the topographic technique had segmentation areas close to the areas of ground truth, but not exactly means that the areas are overlapped. The AOM measure, on other hand, had a higher value for the proposed approach. Because of these characteristics the metrics are analyzed together and not individually.

Most of semi-supervised state-of-the art segmentation techniques uses some kind of adaptive threshold into their algorithm. This can be found in BEMD, BMCS and Wavelet Analysis algorithm. The Topographic Approach, although is based in the concept of concentric regions, also uses threshold in their process. The problem involving threshold based algorithm is that they have difficult to segment low contrast images and specifically ill-defined and

spiculated tumors, because the mass and the tissue have similar values of intensity. For seed based techniques, such as growCut, they usually have a better segmentation for ill-defined and spiculated lesions, but depend on an accurate selection of seeds. The addition of the gaussian fuzzy membership function reduces the need for an accurate selection of seeds, maintaining the quality of segmentation.

Although this work used a gaussian function to map the region of tumor, other functions can be implemented to improve the quality of results. Although the Gaussian region does not have a spiculated shape, it was able provide a good segmentation. The use of specific membership functions for each type of tumor and tissue is also feasible. The automatic generation of seed points also can be improved to deal with images of mammogram with low contrast and dense tissue.

6. Conclusion

In this work we proposed a new approach to segment masses in digital mammography images using an adaptive fuzzy modified version of the general-purpose interactive GrowCut segmentation algorithm. Differently from the classical GrowCut, in which users have to select points internal and external to the object of interest to be segmented, the introduction of a Gaussian fuzzy membership function allows user to select just internal points, trying to add to our algorithm some robustness and fault-tolerance that do not exist in the original approach. Furthermore, in order to minimize the need of specialist human intervention, we used the Differential Evolution optimization algorithm to select automatically these internal points, defining a multi-objective fitness function to guide the process to maximize both the distance between points and the overall brightness of the selected pixels, allowing users to obtain non-collapsing points located inside mammary lesions, regions

usually brighter than other tissues. To automatically identify the best parameters to each ROI, we applied a non-linear regression to define a equation based on the Haralick features of an image. Therefore, the method automatically adapts its parameters according to the features of each image.

In order to evaluate our proposal, we selected 57 lesion images of MiniMIAS mammography database. Results were evaluated taking into account boundaries shapes of segmented lesions. Results obtained with the proposed approach were compared with the following state-of-the-art methods: BEMD, BMCS, LBI, MCW, Topographic Approach, and Wavelet Analysis. Results were considered very good for spiculated and ill-defined lesion images. For circumscribed lesions, results could be considered at least competitive. Therefore, the proposed adaptive semi-supervised Fuzzy GrowCut segmentation algorithm can be considered a feasible and suitable tool to segment masses in digital mammograms, besides having no parameters of configuration.

The main contribution of this work consists of the modification of the evolution rule of GrowCut cellular automata, introducing a Gaussian fuzzy membership function. The use of a Gaussian function combined with the cellular automata evolution rule eliminates the need of selection of external seed points, which is not seen in state-of-art techniques, besides maintaining the quality of segmentation.

This work also contributes with a more fault-tolerant version of GrowCut, because just internal points are selected and used to mount a membership function to establish segmentation boundaries. Furthermore, the proposed approach is based on the center of mass of selected points, making the method more robust.

Results could be extended to other mammography images databases, in case ground-truth images could be obtained in order to evaluate the performance of the proposed semi-supervised segmentation algorithm. However, this is a considerably hard task, once a considerable effort should be made to join a relatively large team of health specialists together in order to mount a reliable ground-truth set of images.

Although our segmentation algorithm was designed to deal with the problem of segmenting masses in digital mammograms, this is not the unique problem our semi-supervised Fuzzy GrowCut algorithm could deal with. As the original GrowCut has been successfully applied to other biomedical image analysis applications [42–44], specifically those based on X-ray computerized tomography and magnetic resonance imaging, due to the similarities with mammography images, we could also use our method for those images, specially those in which segmenting objects of interest with complex boundaries is fundamental to obtain feasible results, like the detection of lung nodules, pancreas segmentation, and measurement of gray matter in magnetic resonance brain imaging. Future works include applying the proposed method to segment tumors in other types of medical images.

References

- [1] World Health Organization, WHO Position Paper on Mammography Screening, 2014, pp. 7–10.
- [2] C.E. DeSantis, C.C. Lin, A.B. Mariotto, R.L. Siegel, K.D. Stein, J.L. Kramer, R. Alteri, A.S. Robbins, A. Jemal, Cancer treatment and survivorship statistics, 2014, CA Cancer J. Clin. 64 (4) (2014) 252–271, <http://dx.doi.org/10.3322/caac.21235>, <http://www.ncbi.nlm.nih.gov/pubmed/24890451>.
- [3] M.P. Coleman, M. Quaresma, F. Berriño, J.M. Lutz, R. De Angelis, R. Capocaccia, P. Bailly, B. Rachet, G. Gatta, T. Hakulinen, A. Micheli, M. Sant, H.K. Weir, J.M. Elwood, H. Tsukuma, S. Koifman, G.A. e Silva, S. Francisci, M. Santaquilani, A. Verdecchia, H.H. Storm, J.L. Young, Cancer survival in five continents: a worldwide population-based study (CONCORD), Lancet Oncol. 9 (8) (2008) 730–756, [http://dx.doi.org/10.1016/S1470-2045\(08\)70179-7](http://dx.doi.org/10.1016/S1470-2045(08)70179-7).
- [4] S.K. Bandyopadhyay, I.K. Maitra, T.H. Kim, Identification of abnormal masses in digital mammography images, in: Proceedings – 2011 International Conference on Ubiquitous Computing and Multimedia Applications, UCMA 2011 (July 2015), 2012, pp. 35–41, <http://dx.doi.org/10.1109/UCMA.2011.16>.
- [5] D.C. Allred, J.M. Harvey, M. Berardo, G.M. Clark, Prognostic and predictive factors in breast cancer by immunohistochemical analysis, Modern Pathol. 11 (2) (1998) 155–168.
- [6] S. Litière, G. Werutsky, I.S. Fentiman, E. Rutgers, M.R. Christiaens, E. Van Limbergen, M.H.A. Baajens, J. Bogaerts, H. Bartelink, Breast conserving therapy versus mastectomy for stage I-II breast cancer: 20 year follow-up of the EORTC 10801 phase 3 randomised trial, Lancet Oncol. 13 (4) (2012) 412–419.
- [7] W.I. Suleiman, S.J. Lewis, D. Georgian-Smith, M.G. Evanoff, M.F. McEntee, Number of mammography cases read per year is a strong predictor of sensitivity, J. Med. Imaging 1 (1) (2014) 155–183, <http://dx.doi.org/10.1117/1.JMI.1.015503>.
- [8] D.X. Wang, F. Yuan, H. Sheng, An algorithm for medical imaging identification based on edge detection and seed filling, in: in: ICCASM 2010–2010 International Conference on Computer Application and System Modeling, Proceedings, vol. 15, 2010, pp. 547–548.
- [9] S.Y.S. Ye, S.Z.S. Zheng, W.H.W. Hao, Medical image edge detection method based on adaptive facet model, in: in: 2010 International Conference on Computer Application and System Modeling (ICCASM), vol. 3, 2010, pp. 574–578, <http://dx.doi.org/10.1109/ICCASM.2010.5620409>.
- [10] V. Raman, P. Sumari, H. Then, S.A.K. Al-Omari, Review on mammogram mass detection by machine learning techniques, Int. J. Comput. Electr. Eng. 3 (6) (2011) 873–879, <http://dx.doi.org/10.7763/IJCEE.2011.V3.436>.
- [11] V. Vezhnevets, V. Konouchine, GrowCut – interactive multi-label N-D image segmentation by cellular automata, Graphicon (2005) 150–156.
- [12] X. Liu, X. Xu, J. Liu, Z. Feng, A new automatic method for mass detection in mammography with false positives reduction by supported vector machine, in: in: 2011 4th International Conference on Biomedical Engineering and Informatics (BMEI), vol. 1, 2011, pp. 33–37, <http://dx.doi.org/10.1109/BMEI.2011.6098328>.
- [13] S.S. Mohamed, G. Behiels, P. Dewaele, Mass candidate detection and segmentation in digitized mammograms, in: in: TIC-STH'09: 2009 IEEE Toronto International Conference – Science and Technology for Humanity, IEEE, 2009, pp. 557–562, <http://dx.doi.org/10.1109/TIC-STH.2009.5444438>.
- [14] G. Ertas, H.O. Gulcur, M. Tunaci, O. Osman, O.N. Ucan, A preliminary study on computerized lesion localization in MR mammography using 3D nMITR maps, multilayer cellular neural networks, and fuzzy c-partitioning, Med. Phys. 35 (1) (2008) 195–205.
- [15] G. Ertas, H.O. Gulcur, M. Tunaci, An interactive dynamic analysis and decision support software for MR mammography, Comput. Med. Imaging Graph. 32 (4) (2008) 284–293.
- [16] G.W. Jiji, J.R. Marsilin, Localization of tumor and its stage using intelligent techniques, Appl. Soft Comput. 27 (2015) 468–473, <http://dx.doi.org/10.1016/j.asoc.2014.10.012>.
- [17] M. Sundaram, K. Ramar, N. Arumugam, G. Prabin, Histogram modified local contrast enhancement for mammogram images, Appl. Soft Comput. 11 (8) (2011) 5809–5816, <http://dx.doi.org/10.1016/j.asoc.2011.05.003>.
- [18] N. Al-Najdawi, M. Biltawi, S. Tedmori, Mammogram image visual enhancement mass segmentation and classification, Appl. Soft Comput. 35 (2015) 175–185, <http://dx.doi.org/10.1016/j.asoc.2015.06.029>.
- [19] A. Oliver, J. Freixenet, J. Martí, E. Pérez, J. Pont, E.R.E. Denton, R. Zwiggelaar, A review of automatic mass detection and segmentation in mammographic images, Med. Image Anal. 14 (2) (2010) 87–110.
- [20] S. Lewis, A. Dong, Detection of breast tumor candidates using marker-controlled watershed segmentation and morphological analysis, in: in: 2012 IEEE Southwest Symposium on Image Analysis and Interpretation (SSIAI), 2012, pp. 1–4, <http://dx.doi.org/10.1109/SSIAI.2012.6202438>.
- [21] M. Eltoukhy, I. Faye, An adaptive threshold method for mass detection in mammographic images, in: in: 2013 IEEE International Conference on Signal and Image Processing Applications (ICSIPA), 2013, pp. 374–378, <http://dx.doi.org/10.1109/ICSIPA.2013.6708036>.
- [22] B.W. Hong, B.S. Sohn, Segmentation of regions of interest in mammograms in a topographic approach, in: in: IEEE Transactions on Information Technology in Biomedicine, vol. 14, IEEE, 2010, pp. 129–139, <http://dx.doi.org/10.1109/TITB.2009.2033269>.
- [23] G.-Y. Dai, Z.-C. Li, J. Gu, L. Wang, X.-M. Li, Segmentation of kidneys from computed tomography using 3d fast growcut algorithm, in: in: 2013 20th IEEE International Conference on Image Processing (ICIP), 2013, pp. 1144–1147, <http://dx.doi.org/10.1109/ICIP.2013.6738236>.
- [24] T. Yamasaki, T. Chen, M. Yagi, T. Hirai, R. Murakami, Comparative study of interactive seed generation for growcut-based fast 3d mri segmentation, in: in: Signal Information Processing Association Annual Summit and Conference (APSIPA ASC), 2012 Asia-Pacific, 2012, pp. 1–4.
- [25] F.R. Cordeiro, W.P. Santos, A.G. Silva-Filho, Segmentation of mammography by applying growcut for mass detection, in: in: Studies in Health Technology and Informatics, vol. 192, 2013, pp. 87–91.
- [26] S.-w. Zheng, J. Liu, C.-C. Liu, A Random-Walk Based Breast Tumors Segmentation Algorithm for Mammograms, 2013, pp. 66–74.
- [27] P. Rahmati, A. Adler, G. Hamarneh, Mammography segmentation with maximum likelihood active contours, Med. Image Anal. 16 (6) (2012) 1167–1186.
- [28] J. Chakraborty, S. Mukhopadhyay, V. Singla, N. Khandelwal, R. Rangayyan, Detection of masses in mammograms using region growing controlled by multilevel thresholding, in: in: 2012 25th International Symposium on Computer-Based Medical Systems (CBMS), 2012, pp. 1–6, <http://dx.doi.org/10.1109/CBMS.2012.6266308>.
- [29] D.C. Pereira, R.P. Ramos, M.Z. do Nascimento, Segmentation and detection of breast cancer in mammograms combining wavelet analysis and genetic algorithms, Comput. Methods Programs Biomed. 114 (1) (2014) 88–101.

- [30] S. Jai-Andaloussi, A. Sekkaki, G. Quellec, M. Lamard, G. Cazuguel, C. Roux, Mass segmentation in mammograms by using Bidimensional Empirical Mode Decomposition BEMD, in: Proceedings of the Annual International Conference of the IEEE Engineering in Medicine and Biology Society, EMBS, 2013, pp. 5441–5444.
- [31] G. Hernandez, H.J. Herrmann, Cellular automata for elementary image enhancement, *Graph. Mod. Image Process.* 58 (1) (1996) 82–89.
- [32] P. Sarkar, A brief history of cellular automata, *ACM Comput. Surv. (CSUR)* 32 (1) (2000) 80–107, <http://dx.doi.org/10.1145/349194.349202>.
- [33] L. Grady, Random walks for image segmentation, *IEEE Trans. Pattern Anal. Mach. Intell.* 28 (11) (2006) 1768–1783.
- [34] S. Vicente, V. Kolmogorov, C. Rother, Graph cut based image segmentation with connectivity priors, in: in: 26th IEEE Conference on Computer Vision and Pattern Recognition, CVPR, 2008.
- [35] S. Das, P.N. Suganthan, Differential evolution: a survey of the state-of-the-art, *IEEE Trans. Evol. Comput.* 15 (1) (2011) 4–31.
- [36] R.M. Haralick, K. Shanmugam, I. Dinstein, Textural features for image classification, *IEEE Trans. Syst. Man Cybern.* 3 (6) (1973).
- [37] B. kishore, R. Vijaya, R. Saha, S. Selvan, Article: using Haralick features for the distance measure classification of digital mammograms, *IJCA Proceedings on International Conference on Advanced Computing and Communication Techniques for High Performance Applications ICACCTHPA 2014* (3) (2015) 17–21.
- [38] J. Suckling, J. Parker, D. Dance, S. Astley, I. Hutt, C. Boggis, I. Ricketts, E. Stamatakis, N. Cerneaz, S. Kok, P. Taylor, D. Betal, J. Savage, The Mammographic Image Analysis Society digital mammogram database (JANUARY 1994) (1994) 375–378 <http://discovery.ucl.ac.uk/102193/>.
- [39] T. Berber, A. Alpkocak, P. Balci, O. Dicle, Breast mass contour segmentation algorithm in digital mammograms, *Comput. Methods Programs Biomed.* 110 (2) (2013) 150–159.
- [40] S. Sharma, P. Khanna, Roi segmentation using local binary image, in: in: 2013 IEEE International Conference on Control System, Computing and Engineering (ICCSCE), 2013, pp. 136–141, <http://dx.doi.org/10.1109/ICCSCE.2013.6719947>.
- [41] D. Rey, M. Neuhäuser, Wilcoxon-signed-rank test, in: in: International Encyclopedia of Statistical Science, Springer, 2011, pp. 1658–1659.
- [42] L. Zhu, I. Kolesov, Y. Gao, R. Kikinis, A. Tannenbaum, An effective interactive medical image segmentation method using fast GrowCut, in: International Conference on Medical Image Computing and Computer Assisted Intervention (MICCAI), 2014, pp. 11–20.
- [43] T. Yamasaki, T. Chen, M. Yagi, T. Hirai, R. Murakami, Growcut-based fast tumor segmentation for 3d magnetic resonance images, in: in: SPIE Medical Imaging, vol. 8314, International Society for Optics and Photonics, 2012, pp. 14–22.
- [44] P. Ghosh, S.K. Antani, L.R. Long, G.R. Thoma, Unsupervised grow-cut: Cellular automata-based medical image segmentation, in: Proceedings – 2011 1st IEEE International Conference on Healthcare Informatics, Imaging and Systems Biology, HISB 2011, 2011, pp. 40–47.